RESEARCH ARTICLE | JULY 23 2024

Gyrokinetic investigation of toroidal Alfvén eigenmode (TAE) turbulence

C. J. Ajay ; Ben McMillan ; Arkaprava Bokshi ; Alessandro di Siena; M. J. Pueschel ; Juan Ruiz Ruiz

AIP Advances 14, 075120 (2024)
https://doi.org/10.1063/5.0216629

Gyrokinetic investigation of toroidal Alfvén eigenmode (TAE) turbulence

Cite as: AIP Advances 14, 075120 (2024); doi: 10.1063/5.0216629
Submitted: 30 April 2024 • Accepted: 29 June 2024 •
Published Online: 23 July 2024

C. J. Ajay,[1,2,a)] Ben McMillan,[1] Arkaprava Bokshi,[3] Alessandro di Siena,[4] M. J. Pueschel,[5,6,7] and Juan Ruiz Ruiz[8]

AFFILIATIONS

[1] Centre for Fusion, Space and Astrophysics, Department of Physics, University of Warwick, CV4 7AL Coventry, United Kingdom
[2] Poel Robotics, Thiruvananthapuram, India
[3] York Plasma Institute, University of York, Heslington York YO10 5DD, United Kingdom
[4] Max Planck Institute for Plasma Physics, Boltzmannstr.2, 85748 Garching, Germany
[5] Dutch Institute for Fundamental Energy Research, 5612 AJ Eindhoven, The Netherlands
[6] Eindhoven University of Technology, 5600 MB Eindhoven, The Netherlands
[7] Department of Physics and Astronomy, Ruhr-Universität Bochum, 44780 Bochum, Germany
[8] Rudolf Peierls Centre for Theoretical Physics, University of Oxford, Oxford OX1 3PU, United Kingdom

[a)] **Author to whom correspondence should be addressed:** ajay.cj@poelrobotics.com

ABSTRACT

Toroidal Alfvén eigenmodes (TAEs) can transport fusion-born energetic particles out of the plasma volume, thereby decreasing plasma self-heating efficiency and possibly damaging reactor walls. Therefore, understanding TAE destabilization and identifying saturation mechanisms are crucial to achieving burning plasma. Here, a fully gyrokinetic study is employed. In the case studied, the primary drive mechanism is identified as the resonance between the magnetic drifts and the TAE, and this is seen to be disrupted by equilibrium flow shear, which can stabilize the mode by rotating it in the poloidal plane. It is found that zonal flows do not play a significant role in the saturation of these TAEs and that there are no saturation mechanisms present in the local gyrokinetic picture, which are able to saturate the mode at physically relevant transport levels in the case of TAE-only turbulence. Instead, we confirm that the global profile flattening of fast-ion density is the key saturation mechanism. The nonlinear excitation of TAEs traveling along the electron diamagnetic direction and its beating with the ion diamagnetic TAE, resulting in large amplitude oscillations that may help detect TAEs more easily in tokamaks, are also reported.

I. INTRODUCTION

Alfvénic modes such as Toroidal Alfvén Eigenmodes (TAEs)[1,2] can be detrimental to tokamak operation as they can transport a significant fast-ion population out of the plasma. In addition to decreasing the thermonuclear alpha population necessary for self-burning, the expelled fast-ions may strike and damage the reactor walls. Hence, a proper understanding of TAE destabilization, damping, and saturation mechanisms is crucial.

Many damping mechanisms, such as continuum damping,[3,4] landau damping,[2,5] radiative damping,[6] finite-orbit width effects,[7] etc., can stabilize TAEs linearly. However, once destabilized, usually by the radial gradient of fast-ion pressure, the level at which TAEs saturate nonlinearly becomes relevant for transport prediction. Fast-ion profile relaxation is one of the obvious ways by which it saturates. Other possible saturation pathways may include trapping of fast-ions by finite amplitude TAEs,[8] nonlinear coupling to other micro-/MHD instabilities, or zonal modes.

Kinetic treatment of fast-ions is necessary to model the fast-ion destabilization of TAEs. Therefore, hybrid codes[9–11] where the background species are treated using MHD equations and the fast-ions are treated kinetically are usually used. However, these codes lack the ability to model certain physics that influence mode saturation, such as the nonlinear coupling[12] between short scale structures associated with the continuum, wave-particle interaction necessary for ion induced scattering of TAEs,[13] trapped particle effects that play an important role in zonal flow structure generation,[14] etc. Hence, a full gyrokinetic formalism may be necessary,[15] such as those given in Refs. 16–18.

In this paper, we explore TAE-only turbulence with the help of both the local[19] and global[20,21] versions of the gyrokinetic code GENE[22] to study the destabilization process and identify the saturation mechanisms. Other works[23–25] have looked at coupled scenarios where complex interactions between drift waves and Alfvénic modes have been found to affect transport properties. Hence, the relevance of studying the simplest case of TAE-only turbulence can be understood in context.

We show the resonance of the magnetic (curvature and ∇B) drift of fast-ions with the TAE in velocity space, which facilitates the destabilization mechanism. The poloidal localization of the destabilization region is shown, and the stabilization of the TAE by $E \times B$ flow shear in medium-high flow-shear tokamaks is discussed. TAEs are found to excite significant zonal flows, but they are not found to play a role in saturation. Global flattening of the profile gradient is identified as the most important saturation mechanism with the help of a global code, and the inadequacy of the local code to predict TAE transport quantitatively is stressed.

This paper is organized as follows: In Sec. II, the simulation setup is explained, followed by linear results on the mode structure and the destabilization mechanism in Sec. III. In Sec. IV, the saturation mechanisms are explored with the help of nonlinear simulations, and finally, the conclusions are presented in Sec. V.

II. SIMULATION SETUP

The GENE simulations use a field-aligned coordinate system,[26] where x is the radial coordinate, $y \propto q_s(x)\chi - \phi$ is the binormal coordinate, and $z = \chi$ the parallel coordinate, with q_s being the safety factor, χ being the straight field line poloidal angle, and ϕ being the toroidal angle. Parallel velocity $v_\parallel$ and magnetic moment μ are the velocity space coordinates.

Two versions of the code, *local* and *global*, are used. The local version assumes radially constant background gradients, making the setup and the physics simpler. The global version allows radially varying background gradients, and, as will be discussed in detail in Sec. IV B, it is necessary to predict the flux levels accurately in the case of TAEs.

Given that the primary motivation behind this work is to study the fundamentals of TAE destabilization and saturation, the parameters are chosen such that a simple TAE-only dominated regime is obtained in our simulations rather than the one taken directly from experiments, which might be a mix of many instabilities. The well studied Cyclone Base Case (CBC)[27] parameters are chosen and then tweaked. A fast-ion species (denoted by subscript f) is added along with electrons (e) and thermal ions (i). Concentric circular flux-surface geometry[28] is considered with an inverse aspect ratio of $\epsilon = x_0/R = 0.18$. Mass ratios of $m_f/m_i = 1$ and $m_e/m_i = 2.5 \times 10^{-4}$, density ratios of $n_f/n_e = 0.01$ and $n_i/n_e = 0.99$, temperature ratios of $T_f/T_i = 100$ and $T_e/T_i = 1$, charge ratios of $q_f/q_i = 1$ and $q_e/q_i = -1$, and a normalized electron pressure of $\beta_e = 0.001$ are considered. Collisions and $\delta B_\parallel$ fluctuations are not included. Fourth-order numerical hyper-diffusion terms[29] $(-\nu_z \partial^4/\partial z^4 - \nu_v \partial^4/\partial v_\parallel^4)$ are added on the right hand side of the gyrokinetic equation, with coefficients $h_z = \nu_z/\Delta z^4 = 3.0$ and $h_v = \nu_v/\Delta v_\parallel^4 = 1.0$ along the parallel and parallel velocity coordinates, respectively.

In the *local* simulations, the inverse of the density or temperature background gradient scale lengths, normalized to the major radius R, is $R/L_{N,f} = 25.0$, $R/L_{N,i} = 0$, $R/L_{N,e} = 0.25$, $R/L_{T,f} = 0$, $R/L_{T,i} = 0$, and $R/L_{T,e} = 0$. A safety factor of $q_0 = 1.4$ and magnetic shear of $\hat{s} = 0.8$ are considered. The default nonlinear simulation has a minimum binormal wavenumber of $k_{y,\min}\rho_i = 0.01$ ($L_y = 628.3\rho_i$), where ρ_i is the thermal ion Larmor radius, the radial box size is $L_x = 125.0\rho_i$, and the velocity space box sizes are $L_{v\parallel} = 3\sqrt{2}v_{th,j}$ ($v_{th,j} = \sqrt{T_{0,j}/m_j}$) and $L_\mu = 12T_{0,j}/B_{0,\text{axis}}$ for each species j. The grid resolutions are $N_x \times N_y \times N_z \times N_{v_\parallel} \times N_\mu = 64 \times 20 \times 32 \times 36 \times 12$. A larger radial box-size simulation with $L_x = 1000\rho_i$ and $N_x = 512$ is also used.

The *global* simulation, centered at $x_0 = 0.5a$, where a is the tokamak minor radius, spans a radial width of $L_x = 62.5\rho_i$, with $\rho^\star = \rho_i/a = 0.0036$. A quadratic q-profile of the form $q(x) = 0.84 + 2.24(x/a)^2$ is considered such that both the safety factor and magnetic shear match those of the local simulations at the center. For practical reasons in GENE related to satisfying quasi-neutrality, an extra electron species labeled *en* is included such that $n_e = 0.99n_0$, $n_{en} = 0.01n_0$, $n_i = 0.99n_0$, and $n_f = 0.01n_0$. The radial background temperature and density profiles are of the form $A_j = \exp[-\kappa_{A,j}\epsilon\Delta A_j \tanh((x - x_0)/(a\Delta A_j))]$, where A_j represents the temperature or density of species j, $\kappa_{A,j}$ denotes the peak gradient, and ΔA_j denotes the radial width of the gradient profile; $\kappa_{n,e} = 0$, $\kappa_{n,en} = 95$, $\kappa_{n,i} = 0$, $\kappa_{n,f} = 95$, $\kappa_{T,e} = \kappa_{T,en} = \kappa_{T,i} = \kappa_{T,f} = 0$, and $\Delta n_{en} = \Delta n_f = 0.05$. The minimum binormal wavenumber is $k_{y,\min}\rho_i = 0.02$ corresponding to the minimum toroidal mode number $n_0 = 2$, and the numerical resolutions are $N_x \times N_y \times N_z \times N_{v_\parallel} \times N_\mu = 48 \times 10 \times 32 \times 36 \times 12$. Krook heat and particle sources (see Ref. 30 for details) are also employed with a source rate of $\gamma_h = \gamma_p = 0.015 v_{th,i}/R$, which is approximately an order of magnitude lower than the maximum growth rate so that the time scale on which the source rate changes the profile is smaller than the characteristic time of turbulence.

III. INVESTIGATING THE DESTABILIZATION MECHANISM USING LINEAR SIMULATIONS

Linear simulations are used to probe the details of the linear TAE mode, including its mode structure, the destabilization mechanism, and ballooning angle dependence. The local results are given in Sec. III A followed by global results in Sec. III B.

A. Local linear results

1. Growth rate, frequency, and mode structure

TAEs are found to be unstable at wavenumbers lower than those where Ion Temperature Gradient (ITG) modes are most unstable in a standard CBC scenario. See Fig. 1 shows the growth rates and frequencies plotted as a function of the binormal wavenumber. The TAE mode frequencies clearly lie within the analytic TAE frequency gap, which is estimated as $3\epsilon|k_\parallel v_A|$ following the study by Fu and Van Dam.[2] The gap is centered at the mid-frequency $\omega_{\text{TAE}} = k_\parallel v_a$. Here, $k_\parallel = 1/(2Rq_0)$ is the parallel wavenumber at

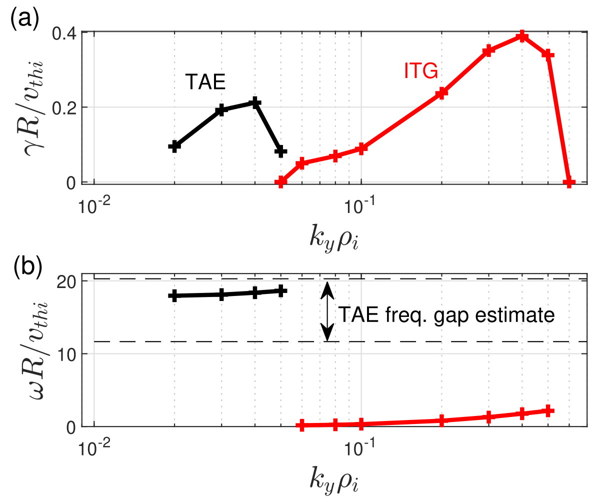

FIG. 1. (a) Growth rate and (b) frequency as a function of binormal wavenumber k_y in linear local simulations. TAE and ITG modes are shown in black and red, respectively.

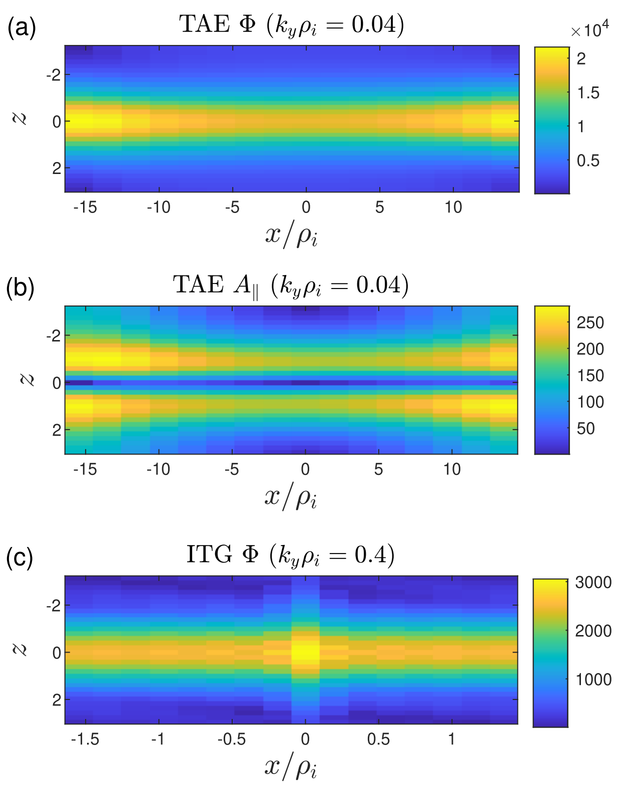

FIG. 2. (a) Electrostatic potential Φ and (b) parallel component $A_\parallel$ of the vector potential plotted on the $x-z$ plane for the TAE mode with $k_y\rho_i = 0.04$. (c) Φ of the ITG mode with $k_y\rho_i = 0.4$.

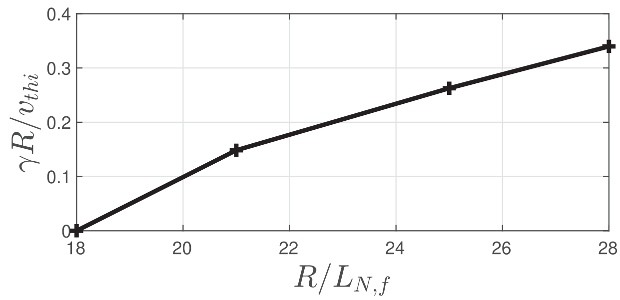

FIG. 3. Growth rate of the TAE ($k_y\rho_i = 0.04$) mode plotted as a function of normalized fast-ion density gradient $\omega_{n,f} = R/L_{N,f}$.

the half-mode-rational surface of intersection of modes with poloidal mode numbers m and m + 1, where $q_s = (2m+1)/2n$ and $v_A = B_0/\sqrt{\mu_0 \sum_j n_j m_j}$ is the Alfvén speed.[31]

The TAE mode has peak amplitude near the half-rational surface, as can be observed in Figs. 2(a) and 2(b), where the electrostatic potential and vector potential are plotted on the $x-z$ plane for the most unstable TAE having $k_y\rho_i = 0.04$. Note that in linear flux-tube GENE simulations, the mode rational surfaces are located at the middle of the radial domain ($x = 0$) and the half-mode-rational surfaces are located at the edges.[32] In contrast, the ITG mode simulated with kinetic electrons has peak amplitude near the mode rational surface,[33,34] as shown in Fig. 2(c).

The default normalized fast-ion density gradient $R/L_{N,f} = 25.0$ is well above the marginal value of $R/L_{N,f} = 18.0$, as can be seen in Fig. 3.

2. Investigating the destabilization mechanism

To investigate the basic destabilization mechanism of TAEs, the method employed by Di Siena *et al.*[24] to study fast-ion stabilization of ITG is used. This involves individually removing terms from the gyrokinetic equation responsible for each of the main physical process.

The relevant gyrokinetic equation in the GENE field aligned coordinates, assuming Maxwellian background distribution function, reads

$$
\begin{aligned}
&-\frac{\partial}{\partial t} f_{1,j} \\
&= \underbrace{\frac{1}{\mathcal{C}}\left[\frac{d\ln n_{o,j}}{dx} + \left(\frac{m_j v_\parallel^2}{2T_{0,j}} + \frac{\mu B_0}{T_{0,j}} - \frac{3}{2}\right)\frac{d\ln T_{o,j}}{dx}\right]\frac{\partial \bar{\Phi}}{\partial y} f_{0,j}}_{\text{background drive}} \\
&+ \underbrace{\frac{\mu B_0 + m_j v_\parallel^2}{m_j \Omega_j}\mathcal{K}_x \Gamma_{x,j}}_{\text{radial magn. drift}} + \underbrace{\frac{\mu B_0 + m_j v_\parallel^2}{m_j \Omega_j}\mathcal{K}_y \Gamma_{y,j}}_{\text{binormal mag. drift}} \\
&+ \underbrace{\frac{\mathcal{C} v_\parallel}{B_0 J^{xyz}}\Gamma_{z,j}}_{\text{parallel advection}} - \underbrace{\frac{\mathcal{C}\mu}{m_j B_0 J^{xyz}}\frac{\partial B_0}{\partial z}\frac{\partial f_{1j}}{\partial v_\parallel}}_{\text{trapping}}, \qquad (1)
\end{aligned}
$$

TABLE I. Growth rate of the $k_y\rho_i$ = 0.04 TAE modes when terms in the gyrokinetic equation are removed.

Terms removed	$\gamma R/v_{th,i}$
None (original)	0.33
Background drive	0
Par. adv. and trap.	0.48
x-curvature	0.31
y-curvature	0

where $\mathcal{C} = B_0/|\nabla x \times \nabla y|$, $\Gamma_{\alpha,j} = \frac{\partial f_{1j}}{\partial \alpha} - \frac{q_j}{m_j v_\parallel}\frac{\partial \bar{\Phi}_1}{\partial \alpha}\frac{\partial f_{0j}}{\partial v_\parallel}$, $\mathcal{K}_x = -\frac{1}{\mathcal{C}}\frac{\gamma_2}{\gamma_1}\frac{\partial B_0}{\partial z}$, $\mathcal{K}_y = \frac{1}{\mathcal{C}}\left(\frac{\partial B_0}{\partial x} - \frac{\gamma_3}{\gamma_1}\frac{\partial B_0}{\partial z}\right)$, $\gamma_1 = g^{xx}g^{yy} - (g^{xy})^2$, $\gamma_2 = g^{xx}g^{yz} - g^{xy}g^{xz}$, $\gamma_3 = g^{xy}g^{yz} - g^{yy}g^{xz}$, $g^{\alpha\beta} = \nabla\alpha \cdot \nabla\beta$, with $\alpha, \beta = x, y, z$, and $\bar{\Phi}$ denotes the gyro-averaged Φ. In the above-mentioned equation, the neoclassical and nonlinear terms have been excluded since they do not affect the evolution of $f_{1,j}$ in the linear flux-tube limit.

The background drive term determines the evolution of the perturbed distribution function due to spatial gradients of the background distribution and appears as a source term. Other terms appear as phase space advection velocity, such as the magnetic (curvature and ∇B) drifts and the parallel motion and trapping terms. The magnetic drifts are further separated into their radial and binormal components. The results are summarized in Table I. Numerical hyperdiffusion is not included in these simulations for simplicity, and hence, the growth rates are slightly off from those shown in Figs. 1 and 3.

As expected, removing the fast-ion background drive term stabilizes the TAE. Removing the fast-ion parallel advection and trapping terms leads to a higher growth rate, indicating that they provide a net stabilizing effect. Radial magnetic drift is found to have little effect on the mode. The most insightful result is the stabilization of the mode in the absence of the fast-ion binormal magnetic drift term, indicating the relevance of this term in TAE destabilization.

As the modes are close to ideal MHD, the parallel electric field is close to zero, and the drive from fast ions is mostly due to the (perpendicular) magnetic drifts, allowing a $\mathbf{J} \cdot E$ energy exchange to the mode ($\mathbf{J}$ and $\mathbf{E}$ being the current and electric field, respectively), but this also requires background pressure gradients. Therefore, net growth requires that both of these terms be positive. This mechanism also mostly involves drifts in the binormal direction, which is the main way the electric field is oriented.

One can obtain better insight into the fast-ion-TAE resonance by visualizing the wave-particle energy transfer in the velocity space. For this purpose, a free-energy based diagnosis[24,35] is used. The total system free energy E in the electrostatic case is defined as

$$E = \sum_j \mathrm{Real}\left[\int dz d\mu dv_\parallel \frac{\pi B_0 n_0 T_0}{2 f_{0,j}} (\Phi^* + f^*_{1,j}) f_{1,j}\right].$$

A free-energy based growth rate γ_j for each species can be obtained such that

$$\gamma = \sum_j \gamma_j = \frac{1}{E}\sum_j \frac{\partial E_j}{\partial t},$$

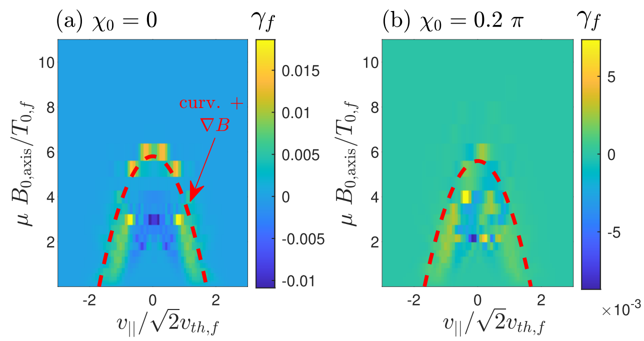

FIG. 4. Fast-ion free-energy based growth rate γ_f plotted on the $v_\parallel - \mu$ velocity plane for ballooning angles (a) χ_0 = 0 and (b) $\chi_0 = 0.2\pi$ for the $k_y\rho_i$ = 0.04 TAE. The red dashed line indicates the magnetic (curvature and ∇B) drift resonance curve.

where $\partial E_j/\partial t$ is essentially obtained by multiplying the gyrokinetic Eq. (1) with $(\Phi^* + f^*_{1,j})$. The fast-ion growth rate is plotted on the $v_\parallel - \mu$ velocity space, as shown in Fig. 4(a).

Considering only the background drive and magnetic drift terms in the gyrokinetic equation for fast-ions, and assuming perturbations (i.e., Φ and $f_{1,f}$) to be of the form $\exp[-i\omega t + ik_x x + ik_y y]$ in Fourier space, the perturbed distribution function $f_{1,f}$ can be expressed as a fraction, where the denominator contains the resonance between the real frequency ω_r of the wave and the fast-ion magnetic drift frequency, which can be expressed as

$$\omega_r = -\frac{\mu B + m_f v_\parallel^2}{q_f B}\kappa_y k_y. \tag{2}$$

For more details, see Eqs. (2)–(8) in Ref. 24. In Fig. 4, this resonance curve is denoted by the red dashed line. One can observe significant fast ion growth rate contribution overlapping with the resonance curve, as shown in Fig. 4(a), confirming that indeed magnetic drifts play a crucial role in the destabilization mechanism.

The significant contributions at $\mu \simeq 3$ inside the resonance curve shown in Fig. 4(a) result from the parallel advection and trapping contribution, which is confirmed by their absence in a similar figure (not shown) corresponding to the simulation where the parallel advection and trapping terms are removed. These terms have a net stabilizing effect, as confirmed in Table I.

3. Ballooning angle dependence

The curvature and ∇B magnetic drifts, which are primarily oriented along the vertical direction ($\approx \mathbf{B}_0 \times \nabla B_0$), can resonantly drive TAEs only at those poloidal locations where the TAE phase fronts (oriented approximately along the poloidal direction) have a significant component along the same vertical direction. More precisely, these correspond to those poloidal locations where the geometric factor κ_y is negative.

In the default case of a zero ballooning angle, i.e., $\chi_0 = 0$ (χ is the straight field line poloidal angle), when the mode is localized at the outboard mid-plane and both the phase fronts and the magnetic drifts are oriented along the same vertical direction, maximum destabilization happens. This is verified in Fig. 5. The growth rate

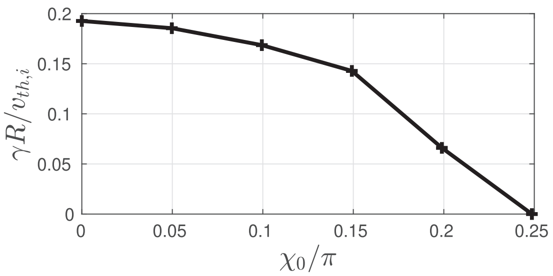

FIG. 5. Linear growth rate of the $k_y\rho_i$ = 0.04 TAE mode as a function of ballooning angle χ_0.

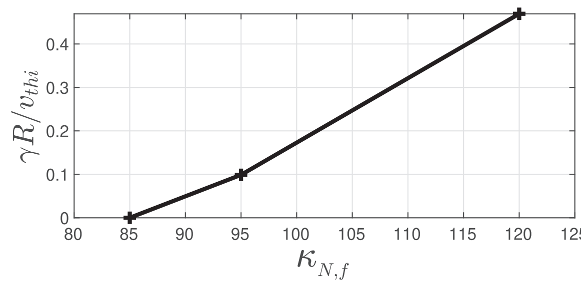

FIG. 7. Growth rate of the global TAE mode as a function of the maximum $\kappa_{N,f}$ of normalized logarithmic fast-ion gradient $\omega_{n,f}$.

is seen to decrease with an increasing ballooning angle, fully stabilizing at $\chi_o = 0.25\pi$. Further evidence can be seen in Fig. 4(b) for the case with a finite ballooning angle of $\chi_0 = 0.2\pi$, where the free-energy based growth rate contributions along the resonance curve can be seen to be mostly destroyed.

B. Global linear results

The fast ion density profile used in global simulations is shown in Fig. 6. In contrast to local simulations, a much higher critical gradient is necessary to destabilize TAEs in global simulations. The growth rate as a function of the peak fast-ion density gradient κ_{nf} is plotted in Fig. 7 for the only unstable mode with $k_y\rho_i = 0.04$ ($n = 4$); modes with other k_y's are stable. The linear mode structure, shown in Fig. 8, peaks near $x = 135\rho_i = 0.48a$ corresponding to safety factor $q = 1.375$, which is the half-rational surface of intersection of the $m = 5$ and $m = 6$ poloidal modes for $n = 4$. Various global effects can explain the higher pressure gradients required for destabilization. For instance, the fast particle drifts may be comparable to the width of the strong pressure gradient region, so the effective drive may be smoothed out. Profile shearing, a reduced TAE continuum gap closer to the magnetic axis (the gap width is proportional to the aspect ratio), etc., are other possibilities.

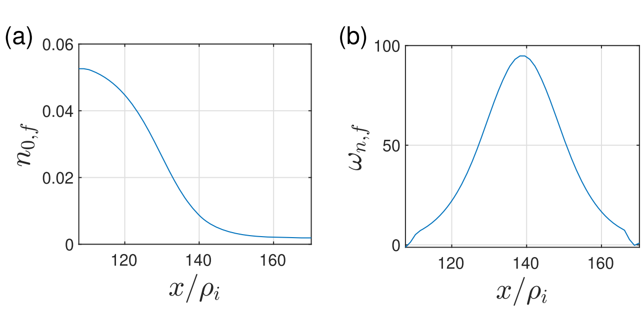

FIG. 6. Background fast-ion (a) density $n_{0,f}$ and (b) normalized logarithmic gradient $\omega_{n,f}$ plotted as a function of the radius in global simulations.

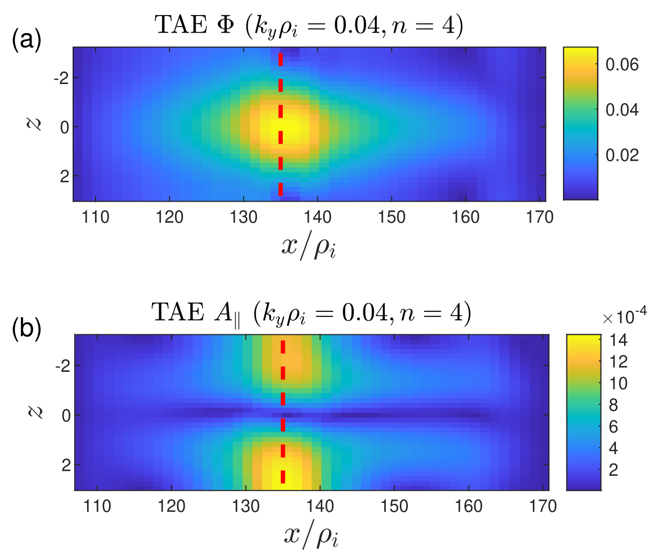

FIG. 8. (a) Φ and (b) $A_\parallel$ plotted on the $x - z$ plane for the global TAE mode with $k_y\rho_i$ = 0.04 and n = 4. The red dashed line indicates the q = 1.375 surface, which is the half-rational surface of intersection of the m = 5 and m = 6 poloidal modes for n = 4.

IV. INVESTIGATING SATURATION MECHANISMS USING NONLINEAR SIMULATIONS

A. Nonlinear local results

Local nonlinear simulations of TAE-only turbulence give much higher heat flux levels than the typical heating power available in tokamaks. See Figs. 9, 12(a), and 13(a) where the fast-ion heat flux time-trace for the default case is plotted in blue; the latter figure is plotted with a higher time resolution. Even when the background fast-ion density gradient is decreased closer to the marginal value, the flux-levels still remain unphysically high, for instance, as shown in Fig. 12(b) in magenta for the case with $R/L_{N,f} = 20$. The fluxes drop to zero once the linear critical gradient at $R/L_{N,f} = 18$ is crossed.

The local simulations have extremely large streamers extending several hundreds of thermal ion Larmor radii. For the default case with a radial box size of $L_x = 125\rho_i$, the streamers extend all through the radial domain, as seen in Fig. 10(a). The flux-tube

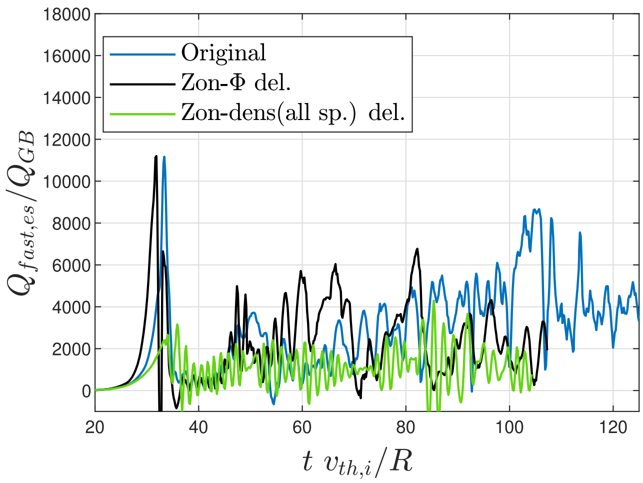

FIG. 9. Fast-ion electrostatic heat flux normalized by the gyro-Bohm value plotted as a function of time in local nonlinear simulations with $L_x = 125\rho_i$. The original simulation is denoted by blue, and the ones with zonal flow (Φ) and zonal density deleted are denoted by black and green, respectively.

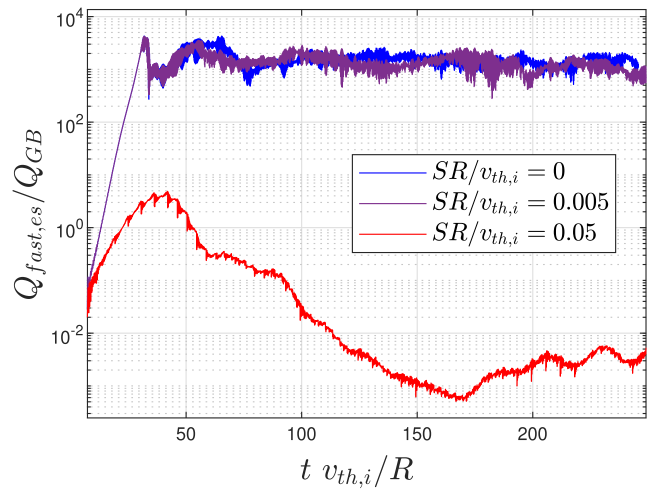

FIG. 11. Fast-ion electrostatic heat flux normalized by the gyro-Bohm value plotted as a function of time in local nonlinear simulations with $L_x = 1000\rho_i$. The original zero flow-shear simulation is denoted by blue. Purple and red correspond to flow-shear rates of $SRv_{th,i} = 0.005$ and 0.05, respectively.

formalism assumes that the radial box-size is larger than the characteristic radial length of turbulent eddies. Hence, to contain the eddies within the radial domain, simulations with a much larger radial box-size of $L_x = 1000\rho_i (> L_y)$ is required, see Fig. 10(b). However, the local (flux-tube) ordering is not well satisfied at such large length scales, and a global approach will be more appropriate. These larger radial box size simulations too give unphysically high heat fluxes, as shown in Fig. 11. Despite the shortcomings of the local model, we can still use these simulations to make certain deductions, as will be discussed in the following.

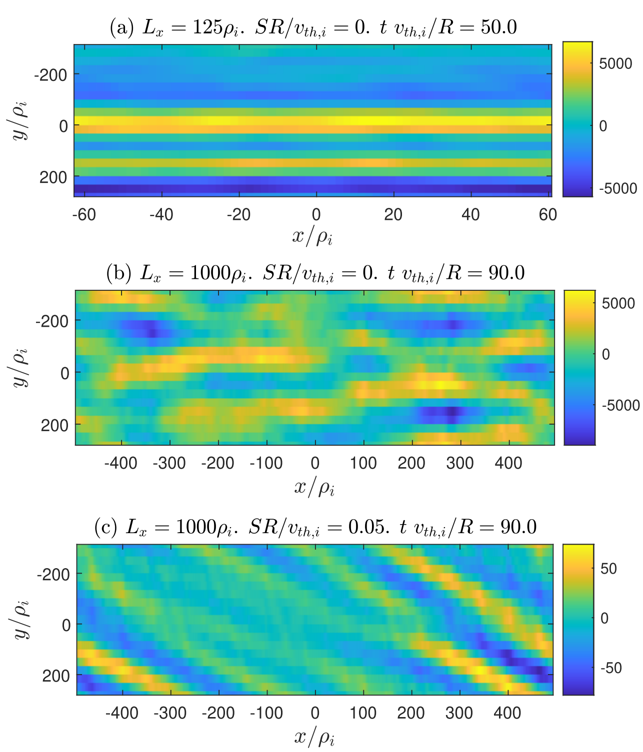

FIG. 10. Electrostatic potential Φ plotted on the $x - y$ plane for the case with a radial box-size of (a) $L_x = 125\rho_i$ and (b) $L_x = 1000\rho_i$, both for the zero background shear-flow (S) case. (c) $L_x = 1000\rho_i$ and $SRv_{th,i} = 0.05$.

Given the low wavenumbers of the unstable TAEs, it is unsurprising that the eddies are radially large; however, other instabilities, such as microtearing modes, which are unstable at similar wavenumbers, have been known to isotropise and saturate to much lower flux levels.[36] This indicates that many of the standard saturation mechanisms, such as that via zonal flows, local profile flattening at rational surfaces, etc., may not be as relevant for TAE turbulence.

1. Role of zonal flows in saturation

Significant zonal flows are driven by TAEs in our simulations; however, they do not play an important role in saturation. To confirm this, simulations with artificially deleted zonal flows are carried out. Much higher heat flux would be expected had zonal flows played an important role in saturation.[37] However, the heat flux-time trace of these simulations, also shown in Fig. 9, is comparable to the original.

2. Role of local profile flattening in saturation

Another mechanism by which turbulence can saturate in flux-tube simulations is by locally flattening the profiles at those radial locations of higher diffusivity. This has been demonstrated for the case of microtearing turbulence[36] where the mode and the corresponding diffusivity are localized near the mode rational surfaces of each toroidal mode, and hence, the zonal T_e perturbations are modified such that the effective (drive) T_e gradient locally flattens significantly at these locations to facilitate saturation. In the case of TAEs, the diffusivity is localized near second order mode rational surfaces; however, the corresponding flattening of fast-ion density

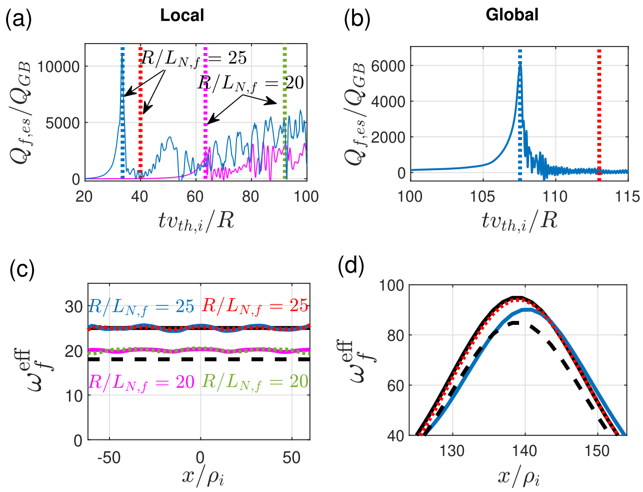

FIG. 12. Fast-ion heat flux plotted as a function of time in (a) local and (b) global simulations. Effective fast-ion density gradient plotted as a function of the radius in (c) local and (d) global simulations at the time instance indicated by the vertical dotted lines in figures (a) and (b), respectively. Solid black lines denote the original background gradients, and dashed lines denote the corresponding linear critical gradients.

at these radial positions is insignificant at only at most 3% of the background density gradient, as shown in Fig. 12(c). The maximum flattening remains less than the critical gradient even in cases closer to the marginal value. Furthermore, the simulation with artificially deleted zonal density perturbations, where the local flattening saturation mechanism would be absent, shown in Fig. 9 using the green trace, does not show much higher heat flux. These results indicate that local profile flattening mechanism is not effective to saturate TAE turbulence.

3. Role of equilibrium flow shear in saturation

$E \times B$ equilibrium flow shear can stabilize TAE turbulence by rotating the mode phase fronts in the poloidal plane, from the outboard mid-plane where the modes are maximally unstable to the unfavorable curvature side (see discussion on ballooning angle dependence in Subsection III A 3). The default case with a radial box size of $L_x = 125\rho_i$ has insufficiently resolved k_x (ballooning angle) modes to properly capture the effects of flow shear,[38] and hence, $L_x = 1000\rho_i$ simulations were used. Simulations with several values of the flow-shear rate S were carried out, where $S = -(r_0/q_0)\,(d\Omega_{\mathrm{tor}}/dx)$, with Ω_{tor} being the toroidal angular velocity. The flow is set to be purely toroidal.[39] The fast-ion heat flux time trace of these simulations is plotted in Fig. 11. While $SRv_{th,i}$ = 0.005 has a negligible effect, $SR/v_{th,i}$ = 0.05 (a realistic value of flow-shear in a typical tokamak) appears to linearly stabilize these TAE modes. However, nonlinear effects could still allow subcritical turbulence.[40] In the time period $t \in [0, 60]v_{th,i}/R$, typical Floquet mode behavior[41,42] can be seen for $SR/v_{th,i}$ = 0.05. During the initial transient growth phase, the modes are radially aligned and can extract energy from fast ions, followed by damping once they are sufficiently tilted. Figure 10(c) shows the tilted mode structure at the end of this time period. These results suggest that flow shear could be an important suppression mechanism for TAE-driven transport of fast ions in medium-high flow-shear tokamaks.

B. Profile flattening in nonlinear global simulation

The relaxation of profile gradients is one of the primary mechanisms by which microturbulence transport in general is quenched. However, in local simulations, which assume the gradients and the resulting flux to be the same across the radius, such a relaxation is not always possible, especially when the modes are elongated along the radius, as already discussed in Sec. IV A. However, there are exceptions, such as, for example, in microtearing instability where the diffusivity is extremely confined near low order rationals and a local flattening at these radial positions can be properly captured even in local simulations.[36]

In global simulations, on the other hand, it is possible to flatten the profiles at those positions where the instability is most unstable, thereby quenching transport. This is observed in TAE global simulations, where unlike in local simulations, the transport is fully quenched, as shown in Fig. 12(b). This emphasizes the need to model TAE turbulence via global codes for proper quantitative predictions.

To demonstrate the global profile flattening, the effective fast-ion density gradient ω_f^{eff} is plotted in Figs. 12(c) and 12(d) for the local and global cases, respectively, as a function of the radius, for two specific times. ω_f^{eff} is the total gradient, defined as the sum of the contributions from the background density gradient and the zonal perturbed density gradient, i.e.,

$$\omega_f^{\mathrm{eff}} = -\frac{dn_{0,f}/dx}{n_{0,f}/R} - \frac{\langle \partial \delta n_f/\partial x\rangle_{yz}}{n_{0,f}/R}.$$

The blue curves shown in Figs. 12(c) and 12(d) correspond to that time when the perturbed amplitudes and heat flux peak [denoted by blue vertical dotted lines in Figs. 12(a) and 12(b)], and there is maximum flattening in the zonal perturbed density gradient. A second curve, red in color, corresponds to a random later time. For the local simulation shown in Figs. 12(a) and 12(c), an additional set of plots, denoted in magenta (and green), is added for a case with $R/L_{N,f}$ = 20, closer to the marginal value.

For the global simulation, the maximum effective gradient, denoted in blue, can be seen to be below the critical gradient, denoted by the dashed black curve, for a significant portion of the radial domain, sufficient enough to stabilize the mode and drop the corresponding flux-levels to zero. The effective gradient, in fact, reduces by a maximum of 15% from the default value denoted by the solid black curve. For the corresponding local simulations, there is only a maximum of 3% flattening; the effective gradient remains well above the critical gradient, and hence, the profile flattening saturation mechanism is not being properly captured.

C. Beating of TAEs traveling along the ion and electron diamagnetic directions

Another interesting observation in TAE turbulence is the intense beating of counter-propagating TAEs in the ion and electron diamagnetic directions. This is illustrated in Fig. 13. In figures (a) and (b), the zoomed fast-ion heat flux as it transitions from an initial linear phase to the nonlinear phase is plotted for the local and global simulations, respectively. In the linear phase, only that

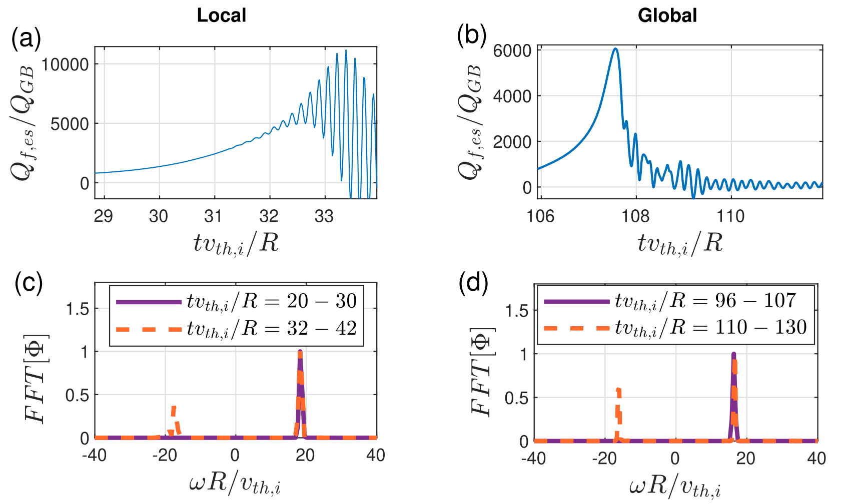

FIG. 13. Fast-ion heat flux in (a) local and (b) global simulations, zoomed near the linear-nonlinear transition. The fast Fourier transformed electrostatic potential in the linear and nonlinear phases are plotted in violet and orange colors, respectively, for (c) local and (d) global simulations.

TAE traveling along the ion diamagnetic direction is made unstable by the resonance of the fast-ion magnetic (curvature and ∇B) drift with the TAE. This is confirmed in Figs. 13(c) and 13(d), where the fast Fourier transform of the electrostatic potential only has peaks on the positive frequency side corresponding to the ion-diamagnetic direction, as per GENE convention. However, once the simulation reaches the nonlinear phase, significant oscillations can be seen on the fast-ion fluxes and other perturbed quantities, having a frequency equal to that of the most unstable TAE. This essentially results from the nonlinear excitation of the electron diamagnetic direction TAE and the subsequent beating with the ion-diamagnetic one. This too is verified in Figs. 13(c) and 13(d), where the Fourier transform has peaks both in the positive and negative frequencies. The beating results in high amplitude oscillations in flux surface quantities, which might potentially be directly observed in diagnostics. External magnetic diagnostics are often able to resolve the direction of mode propagation, and this phenomenon would be seen as comparable magnitudes in the positive- and negative-propagating mode.

V. CONCLUSIONS

Gyrokinetic simulations of TAE turbulence were carried out to study the fast-ion destabilization and saturation mechanisms. With the help of free-energy based diagnostics, the destabilization mechanism has been demonstrated to involve the resonance of magnetic drift of fast-ions with the TAE mode. This resonance is more destabilizing at the outboard midplane, and hence, when the mode gets rotated in the poloidal plane by equilibrium flow shear, it is stabilized. Our simulations predict that TAE turbulence is low or insignificant in medium-high flow-shear tokamaks. Saturation mechanisms such as that via zonal flows and local profile flattening are shown to be less effective, and local codes are found to give unphysical transport levels. Global profile flattening, on the other hand, is shown to be an important saturation mechanism, and therefore, the necessity for global codes to quantitatively predict fluxes resulting from TAE turbulence is identified. The nonlinear excitation of electron diamagnetic direction TAEs and their beating with the ion-diamagnetic TAEs, producing large oscillations in observable quantities, are also reported.

ACKNOWLEDGMENTS

This research was funded in whole or in part by the Engineering and Physical Sciences Research Council (EPSRC), EP/R034737/1. For the purpose of open access, the author has applied a Creative Commons Attribution (CC BY) licence to any author accepted manuscript version arising from this submission. We acknowledge the CINECA award under the ISCRA initiative, for the availability of high performance computing resources and support. A. Bokshi would like to acknowledge funding through UKRI Grant Nos. EP/R034737/1 and EP/X035336/1, allowing time and access to the ARCHER2 UK National Supercomputing Service (https://www.archer2.ac.uk).

AUTHOR DECLARATIONS

Conflict of Interest

The authors have no conflicts to disclose.

Author Contributions

C. J. Ajay: Conceptualization (equal); Formal analysis (equal); Investigation (equal); Methodology (equal); Visualization (equal); Writing – original draft (equal); Writing – review & editing (equal). **Ben McMillan**: Conceptualization (equal); Funding acquisition (equal); Investigation (equal); Methodology (equal); Project administration (equal); Resources (equal); Supervision (equal); Writing – original draft (equal); Writing – review & editing (equal). **Arkaprava Bokshi**: Formal analysis (equal); Investigation (equal); Resources (equal); Writing – review & editing (equal). **Alessandro di Siena**:

Formal analysis (equal); Investigation (equal); Methodology (equal); Writing – review & editing (equal). **M. J. Pueschel**: Investigation (equal); Writing – review & editing (equal). **Juan Ruiz Ruiz**: Writing – review & editing (equal).

DATA AVAILABILITY

The data that support the findings of this study are available from the corresponding author upon reasonable request.

REFERENCES

[1] C. Z. Cheng and M. S. Chance, "Low-n shear Alfvén spectra in axisymmetric toroidal plasmas," Phys. Fluids **29**(11), 3695–3701 (1986).
[2] G. Y. Fu and J. W. Van Dam, "Excitation of the toroidicity-induced shear Alfvén eigenmode by fusion alpha particles in an ignited tokamak," Phys. Fluids B **1**(10), 1949–1952 (1989).
[3] F. Zonca and L. Chen, "Resonant damping of toroidicity-induced shear-Alfvén eigenmodes in tokamaks," Phys. Rev. Lett. **68**, 592–595 (1992).
[4] H. L. Berk, J. W. Van Dam, Z. Guo, and D. M. Lindberg, "Continuum damping of low-n toroidicity-induced shear Alfvén eigenmodes," Phys. Fluids B **4**(7), 1806–1835 (1992).
[5] R. Betti and J. P. Freidberg, "Stability of Alfvén gap modes in burning plasmas," Phys. Fluids B **4**(6), 1465–1474 (1992).
[6] R. R. Mett and S. M. Mahajan, "Kinetic theory of toroidicity-induced Alfvén eigenmodes," Phys. Fluids B **4**(9), 2885–2893 (1992).
[7] T. Fülöp, M. Lisak, Ya. I. Kolesnichenko, and D. Anderson, "Finite orbit width stabilizing effect on toroidal Alfvén eigenmodes excited by passing and trapped energetic ions," Plasma Phys. Controlled Fusion **38**(6), 811 (1996).
[8] Y. Todo, T. Sato, K. Watanabe, T. H. Watanabe, and R. Horiuchi, "Magne tohydrodynamic Vlasov simulation of the toroidal Alfvén eigenmode," Phys. Plasmas **2**(7), 2711–2716 (1995).
[9] Y. Todo and T. Sato, "Linear and nonlinear particle-magnetohydrodynamic simulations of the toroidal Alfvén eigenmode," Phys. Plasmas **5**(5), 1321–1327 (1998).
[10] G. Y. Fu, W. Park, H. R. Strauss, J. Breslau, J. Chen, S. Jardin, and L. E. Sugiyama, "Global hybrid simulations of energetic particle effects on the $n = 1$ mode in tokamaks: Internal kink and fishbone instability," Phys. Plasmas **13**(5), 052517 (2006).
[11] X. Wang, S. Briguglio, L. Chen, C. Di Troia, G. Fogaccia, G. Vlad, and F. Zonca, "An extended hybrid magnetohydrodynamics gyrokinetic model for numerical simulation of shear Alfvén waves in burning plasmas," Phys. Plasmas **18**(5), 052504 (2011).
[12] L. Chen and F. Zonca, "Gyrokinetic theory of parametric decays of kinetic Alfvén waves," Europhys. Lett. **96**(3), 35001 (2011).
[13] T. S. Hahm and L. Chen, "Nonlinear saturation of toroidal Alfvén eigenmodes via ion Compton scattering," Phys. Rev. Lett. **74**, 266–269 (1995).
[14] L. Chen and F. Zonca, "Nonlinear excitations of zonal structures by toroidal Alfvén eigenmodes," Phys. Rev. Lett. **109**, 145002 (2012).
[15] Z. Qiu, L. Chen, and F. Zonca, "Gyrokinetic theory of toroidal Alfvén eigenmode saturation via nonlinear wave–wave coupling," Rev. Mod. Plasma Phys. **7**(1), 28 (2023).
[16] A. Mishchenko, R. Hatzky, and A. Könies, "Global particle-in-cell simulations of Alfvénic modes," Phys. Plasmas **15**(11), 112106 (2008).
[17] A. Mishchenko, A. Könies, and R. Hatzky, "Global particle-in-cell simulations of fast-particle effects on shear Alfvén waves," Phys. Plasmas **16**(8), 082105 (2009).
[18] J. Lang, Y. Chen, S. E. Parker, and G.-Y. Fu, "Gyrokinetic δf particle simulations of toroidicity-induced Alfvén eigenmode," Phys. Plasmas **16**(10), 102101 (2009).
[19] B. Scott, "Global consistency for thin flux tube treatments of toroidal geometry," Phys. Plasmas **5**(6), 2334–2339 (1998).
[20] T. Görler, X. Lapillonne, S. Brunner, T. Dannert, F. Jenko, F. Merz, and D. Told, "The global version of the gyrokinetic turbulence code gene," J. Comput. Phys. **230**(18), 7053–7071 (2011).
[21] T. Görler, "Multiscale effects in plasma microturbulence," Ph.D. thesis, Universität Ulm, 2009.
[22] F. Jenko, W. Dorland, M. Kotschenreuther, and B. N. Rogers, "Electron temperature gradient driven turbulence," Phys. Plasmas **7**(5), 1904–1910 (2000).
[23] A. Di Siena, T. Görler, H. Doerk, E. Poli, and R. Bilato, "Fast-ion stabilization of tokamak plasma turbulence," Nucl. Fusion **58**(5), 054002 (2018).
[24] A. Di Siena, T. Görler, E. Poli, R. Bilato, H. Doerk, and A. Zocco, "Resonant interaction of energetic ions with bulk-ion plasma micro-turbulence," Phys. Plasmas **26**(5), 052504 (2019).
[25] A. Biancalani, A. Bottino, A. Di Siena, Ö. Gürcan, T. Hayward-Schneider, F. Jenko, P. Lauber, A. Mishchenko, P. Morel, I. Novikau, F. Vannini, L. Villard, and A. Zocco, "Gyrokinetic investigation of Alfvén instabilities in the presence of turbulence," Plasma Phys. Controlled Fusion **63**(6), 065009 (2021).
[26] M. A. Beer, S. C. Cowley, and G. W. Hammett, "Field-aligned coordinates for nonlinear simulations of tokamak turbulence," Phys. Plasmas **2**(7), 2687–2700 (1995).
[27] A. M. Dimits, G. Bateman, M. A. Beer, B. I. Cohen, W. Dorland, G. W. Hammett, C. Kim, J. E. Kinsey, M. Kotschenreuther, A. H. Kritz, L. L. Lao, J. Mandrekas, W. M. Nevins, S. E. Parker, A. J. Redd, D. E. Shumaker, R. Sydora, and J. Weiland, "Comparisons and physics basis of tokamak transport models and turbulence simulations," Phys. Plasmas **7**(3), 969–983 (2000).
[28] X. Lapillonne, S. Brunner, T. Dannert, S. Jolliet, A. Marinoni, L. Villard, T. Görler, F. Jenko, and F. Merz, "Clarifications to the limitations of the s-α equilibrium model for gyrokinetic computations of turbulence," Phys. Plasmas **16**(3), 032308 (2009).
[29] M. J. Pueschel, T. Dannert, and F. Jenko, "On the role of numerical dissipation in gyrokinetic Vlasov simulations of plasma microturbulence," Comput. Phys. Commun. **181**(8), 1428–1437 (2010).
[30] X. Lapillonne, B. F. McMillan, T. Görler, S. Brunner, T. Dannert, F. Jenko, F. Merz, and L. Villard, "Nonlinear quasisteady state benchmark of global gyrokinetic codes," Phys. Plasmas **17**(11), 112321 (2010).
[31] W. W. Heidbrink, "Basic physics of Alfvén instabilities driven by energetic particles in toroidally confined plasmas," Phys. Plasmas **15**(5), 055501 (2008).
[32] C. J. Ajay, "Studying the effect of non-adiabatic passing electron dynamics on microturbulence self-interaction in fusion plasmas using gyrokinetic simulations," Ph.D. thesis, École Polytechnique Fédérale de Lausanne, 2020.
[33] J. Dominski, S. Brunner, T. Görler, F. Jenko, D. Told, and L. Villard, "How non-adiabatic passing electron layers of linear microinstabilities affect turbulent transport," Phys. Plasmas **22**(6), 062303 (2015).
[34] C. J. Ajay, S. Brunner, B. McMillan, J. Ball, J. Dominski, and G. Merlo, "How eigenmode self-interaction affects zonal flows and convergence of tokamak core turbulence with toroidal system size," J. Plasma Phys **86**(5), 905860504 (2020).
[35] A. Bañón Navarro, P. Morel, M. Albrecht-Marc, D. Carati, F. Merz, T. Görler, and F. Jenko, "Free energy balance in gyrokinetic turbulence," Phys. Plasmas **18**(9), 092303 (2011).
[36] C. J. Ajay, B. F. McMillan, and M. J. Pueschel, "On the impact of temperature gradient flattening and system size on heat transport in microtearing turbulence," Nucl. Fusion **63**(6), 066024 (2023).
[37] Z. Lin, T. S. Hahm, W. W. Lee, W. M. Tang, and R. B. White, "Turbulent transport reduction by zonal flows: Massively parallel simulations," Science **281**(5384), 1835–1837 (1998).
[38] B. F. McMillan, J. Ball, and S. Brunner, "Simulating background shear flow in local gyrokinetic simulations," Plasma Phys. Controlled Fusion **61**(5), 055006 (2019).
[39] D. Told, "Gyrokinetic microturbulence in transport barriers," Ph.D. thesis, Universität Ulm, 2012.
[40] F. J. Casson, A. G. Peeters, Y. Camenen, W. A. Hornsby, A. P. Snodin, D. Strintzi, and G. Szepesi, "Anomalous parallel momentum transport due to $E \times B$ flow shear in a tokamak plasma," Phys. Plasmas **16**(9), 092303 (2009).
[41] R. E. Waltz, R. L. Dewar, and X. Garbet, "Theory and simulation of rotational shear stabilization of turbulence," Phys. Plasmas **5**, 1784 (1998).
[42] V. I. Dagnelie, J. Citrin, F. Jenko, M. J. Pueschel, T. Görler, D. Told, and H. Doerk, "Growth rates of ITG modes in the presence of flow shear," Phys. Plasmas **26**(1), 012502 (2019).